Bachelor's Thesis

# Optimization of EV Suspension Parameters Using Data-Driven Surrogate Modeling

School of Mechanical and Control Engineering

Handong Global University

Dongjun Han, Youngkeun Kim*

# Table of Contents

**Extended Abstract**

# Optimization of EV Suspension Parameters Using Data-Driven Surrogate Modeling

## 1. Introduction

This research proposes a data-driven suspension optimization framework for electric vehicles competing in the KSAE Smart e-Mobility Competition. The endurance race within this event presents a technical challenge involving both high-speed and sharp-cornering segments, where vehicle handling performance, especially during cornering, plays a critical role in minimizing lap time.

Suspension systems govern key aspects of vehicle dynamics, including tire contact, load transfer, and stability. However, traditional tuning methods—based on empirical rules or trial-and-error—are inefficient and inadequate for capturing nonlinear and high-dimensional behaviors inherent in real driving scenarios. Furthermore, handling stability and ride comfort often exhibit a trade-off relationship, requiring a balanced, objective-driven optimization strategy.

To address these challenges, this study focuses on six suspension parameters: front/rear spring stiffness, compression damping, and rebound damping. A multi-objective optimization approach is adopted, prioritizing handling (weight: 0.8) over comfort (weight: 0.2), aligned with competition demands. Gaussian Process Regression (GPR) is employed to build surrogate models based on a limited number of simulation and experimental samples, enabling efficient exploration of the design space without relying on exhaustive physical testing.

By integrating vehicle dynamics insights with surrogate modeling techniques, this research contributes a scalable and performance-driven methodology for suspension design tailored to competitive e-mobility applications.

## 2. Methodology

This study employs a hybrid methodology combining theoretical vehicle dynamics, simulation data generation, and experimental validation to optimize suspension parameters for improved handling performance.

First, a simplified multi-body dynamics model of the vehicle is developed to capture key ride and

handling behaviors, including pitch, roll, heave, lateral, and yaw motions. These dynamic insights are then implemented in a simulation environment to generate performance response data for various suspension parameter sets. The six design variables include front and rear spring stiffness, compression damping, and rebound damping coefficients.

Using this simulation data, a Gaussian Process Regression (GPR) model is trained to serve as a surrogate model that predicts key performance indicators such as roll angle, lateral acceleration, and heave vibration. This simulation-based surrogate enables efficient exploration of the design space while reducing computational cost.

In parallel, an experiment-based surrogate model is constructed using vibration response data collected from physical vehicle testing. A test vehicle equipped with IMU sensors captures real-world pitch, roll, and vertical acceleration responses under controlled cornering maneuvers. This experimental data is used to train a second GPR model that reflects actual vehicle behavior under dynamic loads.

Together, these two surrogate models—simulation-based and experiment-based—allow for comparative analysis and multi-objective optimization. Handling and comfort are evaluated using weighted scoring functions derived from both modeling approaches, ultimately guiding the selection of optimal suspension parameter sets that improve cornering performance without significantly compromising ride comfort.

## 3. Results and Discussion

The proposed suspension optimization framework was validated through both simulation- and experiment-based surrogate models. Pareto front analysis revealed that high spring stiffness consistently improved both handling and comfort, making it a robust design choice across different weightings. In contrast, damping parameters showed divergent trends: simulation results favored lower damping for handling, while experimental results showed minimal sensitivity, likely due to noise and measurement limitations.

At the target weight ratio (handling:comfort = 0.8:0.2), the optimized configuration achieved a +64% total performance improvement over the baseline, primarily driven by increased spring stiffness and reduced damping. This confirms the surrogate model's effectiveness in identifying high-performing parameter sets under idealized assumptions.

However, experimental surrogate models showed overconfidence and underestimated uncertainty, particularly for damping effects. This highlights the need for improved data fidelity, signal processing, and expanded testing. Future work should explore enhanced modeling approaches and more rigorous experiments to bridge the gap between simulation and real-world applicability.

# 1. Introduction

## 1.1 Background and Motivation

The KSAE Smart e-Mobility Competition is a prominent annual event that challenges university teams to design and optimize electric vehicles capable of demonstrating high performance across various driving scenarios. Among the key stages of the competition is the endurance race, which involves a technical track characterized by both high-speed straight segments and sharp cornering zones. To minimize lap times in such conditions, vehicle dynamics during cornering becomes a dominant performance factor.

Suspension systems play a critical role in shaping vehicle dynamics, as they directly influence the car's ability to maintain tire contact, manage load transfer, and preserve stability during high-speed maneuvers. However, the tuning of suspension parameters, including spring stiffness and damping characteristics, has traditionally relied on empirical knowledge and iterative trial-and-error processes. This approach is not only time-consuming and resource-intensive but also limited in its ability to reflect complex nonlinear behaviors encountered in real-world driving environments.

Furthermore, the dual objectives of maximizing handling stability and ensuring ride comfort often exist in a trade-off relationship. Stiffer setups improve handling performance but at the cost of increased ride harshness, while softer configurations improve comfort but degrade vehicle responsiveness and cornering capability. Given the competition's emphasis on reducing lap time and navigating sharp turns with precision, handling stability is prioritized override comfort in this study.

## 1.2 Research Objective and Scope

The primary objective of this research is to optimize the suspension parameters of an electric vehicle designed for the KSAE Smart e-Mobility Competition, with a particular focus on enhancing handling performance during cornering. To this end, a set of key design variables are considered, including:

$$K_{front}, K_{rear}, C_{COMP_{front}},$$

$$C_{COMP_{rear}}, C_{REB_{front}}, C_{REB_{rear}}$$

where $K$ represents spring stiffness, and $C_{COMP}$ and $C_{REB}$ denote the compression and rebound damping coefficients, respectively. The optimization process adopts a multi-objective framework with a weighted preference of 0.8 for handling stability and 0.2 for ride comfort, reflecting the specific performance requirements of the competition track.

To address the limitations of traditional tuning methods, this study employs data-driven surrogate modeling techniques to efficiently explore the design space and reduce the reliance on costly physical experiments. By constructing both simulation-based and experiment-based surrogate models, we aim to predict vehicle dynamic responses and identify optimal parameter sets that deliver high handling stability without compromising essential ride comfort.

## 1.3 Contribution of This Study

Previous research on suspension system optimization has predominantly relied on empirical parameter tuning or full-factorial grid sampling techniques. For instance, Kim et al. (2016) employed a comprehensive grid-based sampling method to optimize spring and damper configurations for the Korean PRT (Personal Rapid Transit) vehicle. While this approach allowed systematic coverage of the design space, it suffered from severe combinatorial explosion, rendering the method inefficient and costly when extended to more complex vehicle models or larger parameter sets. Moreover, its applicability was constrained to simplified scenarios, limiting its effectiveness in capturing dynamic vehicle behavior under realistic conditions.

A broader review of related literature reveals a similar trend. Many prior studies depend on simulation environments such as Adams or CarSim, which operate under fixed-input assumptions and struggle to represent nonlinear

dynamics accurately. Key vehicle responses such as tire behavior, load transfer, and road surface variability are either idealized or excluded, resulting in models that lack robustness and real-world adaptability. Furthermore, the absence of surrogate modeling frameworks in many of these studies has restricted the potential for rapid design iterations and informed trade-off analysis.

To address these limitations, the present study adopts a data-driven, surrogate-model-based approach to suspension parameter optimization. Specifically, this research integrates Gaussian Process Regression (GPR) to construct predictive models from a limited number of simulation and experimental samples. By employing sample-efficient design of experiments, the study aims to overcome the inefficiencies of grid sampling while maintaining high predictive accuracy.

This surrogate modeling strategy enables the simultaneous consideration of handling stability and ride comfort, offering a practical path toward multi-objective optimization. It not only reduces the computational and experimental burden but also enhances the adaptability of the model to nonlinear and dynamic behavior observed during real-world driving. In doing so, this study contributes a more efficient, flexible, and performance-driven methodology for vehicle suspension design tailored to competitive mobility applications.

## 1.4 Optimization Strategy Comparison

While Section 1.2 introduced the key suspension design variables, this section focuses on the complexity that arises when optimizing them simultaneously. The interaction of six variables, including front/rear spring stiffness and damping coefficients—forms a high-dimensional, nonlinear design space that traditional tuning methods struggle to navigate efficiently. Each of these variables contributes nonlinearly to dynamic behaviors such as roll angle, pitch angle, lateral acceleration, and heave, making manual or empirical tuning not only time-consuming but also unreliable in terms of consistency and completeness.

Traditional tuning processes often rely on empirical knowledge, repeated physical testing, and rule-of-thumb heuristics. While these methods may yield acceptable results in limited scenarios, they fall short when the goal is to understand and optimize high-dimensional, nonlinear interactions systematically. Especially as the number of parameters increases, the design space becomes exponentially more complex, and traditional methods struggle to account for trade-offs between conflicting objectives—such as handling and comfort—without incurring excessive cost and effort.
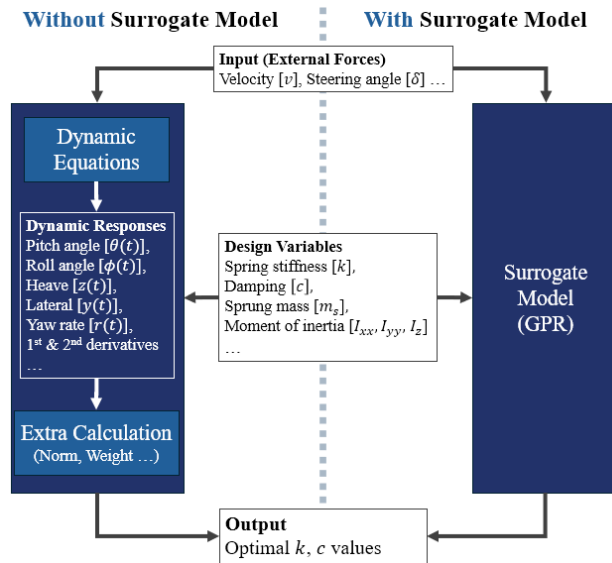


**Fig. 1. Comparison of Optimization Workflows With and Without Surrogate Modeling**

In contrast, the surrogate model-based approach allows for efficient navigation of this complex space. Once trained, the surrogate model—based on Gaussian Process Regression (GPR)—can rapidly estimate vehicle responses across a wide range of design combinations, enabling informed decisions without repeated simulations or physical tests. This is particularly valuable in high-dimensional optimization problems where the computational cost of exhaustive evaluation is prohibitive.

As illustrated in **Figure 1**, surrogate modeling transforms the optimization process by serving as a functional shortcut between input variables and vehicle performance outputs. It replaces the need for repeated testing or simulations with fast, predictive inference, thus enabling efficient multi-objective design optimization.

# 2. Methodology

## 2.1 Dynamics Analysis – Theoretical Framework

To build a meaningful and interpretable surrogate model for suspension optimization, it is essential to first understand the underlying vehicle dynamics that govern ride and handling responses. This study begins with a systematic analysis of the dynamic behavior of a ground vehicle under cornering maneuvers, focusing on pitch, roll, heave, lateral, and yaw motions—all of which are significantly influenced by the suspension system.

The dynamic response of a vehicle is inherently governed by a complex interplay of mechanical subsystems, including mass distribution, inertia, damping, and external forces. Cornering induces nonlinear effects such as lateral acceleration, load transfer, and suspension compression, all of which contribute to changes in body posture and tire contact conditions. While high-fidelity simulations or physical experiments may capture these behaviors, they often involve substantial computational or experimental costs, making them unsuitable for iterative optimization tasks.

To address this, a set of simplified dynamic equations is adopted as a foundational model. These equations describe the motion of the vehicle body in response to external excitations, under small-angle linearized assumptions. By isolating degrees of freedom such as pitch rate, roll angle, vertical displacement, and yaw rate, the framework allows for the quantification of how suspension parameters impact dynamic stability and ride comfort.

Each dynamic equation reflects a distinct aspect of vehicle behavior:

- Pitch and roll dynamics govern body attitude under acceleration and turning.

- Heave dynamics relate to vertical vibration and ride smoothness.

- Lateral dynamics and yaw rate equations describe vehicle path stability during directional changes.

- Power Spectral Density (PSD) analysis is employed to characterize the frequency content of vehicle accelerations, offering an objective measure for evaluating comfort levels.

This analytical formulation serves as the basis for interpreting both simulation and experimental data and highlights the complexity and coupling effects that make direct analytical optimization impractical. These limitations reinforce the value of surrogate modeling as a viable approach to capturing the essential dynamics without incurring prohibitive cost or computational effort.

### 2.1.1 Fundamental Principle: Newton–Euler Rotational Dynamics

The rotational dynamics of a vehicle during acceleration, braking, and cornering can be modeled using the Newton–Euler formulation, which states that:

$$Moment\ of\ Inertia \\ \times Angular\ Acceleration \\ = External\ Moment - Restoring\ Moment$$

This principle provides the foundation for analyzing pitch and roll motions, both of which are critical to understanding how suspension parameters influence vehicle stability and body control.

### 2.1.2 Pitch Dynamics Equation (Longitudinal Tilting)

The pitch dynamics equation describes the vehicle's angular motion about the lateral axis, which becomes prominent during longitudinal acceleration or braking. The equation is given by:

$$I_{yy} \cdot \ddot{\theta}(t) = M_\theta(t) - (k_f a^2 + k_r b^2) \cdot \theta(t) \\ - (c_f a^2 + c_r b^2) \cdot \dot{\theta}(t)$$

- $M_\theta(t)$: Represents the external pitch moment induced by longitudinal forces (e.g., acceleration or braking).

- $k_f a^2 + k_r b^2$: Corresponds to the restoring moment due to spring stiffness acting at

distances $a$ and $b$ from the vehicle's center of gravity (CG) to the front and rear suspension points.

- $c_f a^2 + c_r b^2$: Denotes the damping moment generated in response to pitch angular velocity.

This formulation captures the interplay between inertial response and suspension-induced restoring/damping forces in pitch motion.

### 2.1.3 Roll Dynamics Equation (Lateral Tilting)

The roll dynamics equation captures the angular motion about the longitudinal axis, which is primarily influenced by lateral acceleration during cornering. It is expressed as:

$$I_{xx} \cdot \ddot{\phi}(t) = M_\phi(t) - (k_f t_f^2 + k_r t_r^2) \cdot \phi(t) - (c_f t_f^2 + c_r t_r^2) \cdot \dot{\phi}(t)$$

- $M_\phi(t)$: Denotes the roll moment resulting from lateral acceleration forces.

- $t_f, t_r$: Represent the track widths from the CG to the left and right suspension attachment points at the front and rear, respectively.

- The remaining terms mirror the structure of the pitch equation, with distance terms $a, b$ replaced by $t_f, t_r$ to reflect lateral symmetry.

Both pitch and roll dynamic models provide a simplified yet physically meaningful representation of the rotational behavior of the vehicle body. These equations are essential for assessing how suspension design parameters, such as stiffness and damping distribution, affect the vehicle's ability to resist tilting motions and maintain composure under dynamic load transfers.

### 2.1.4 Heave Dynamics Equation

The heave motion refers to the vertical displacement of the vehicle's center of gravity (CG) due to suspension deflection under load. The corresponding dynamic model is expressed as:

$$m_s \cdot \ddot{z}(t) + (c_f + c_r) \cdot \dot{z}(t) + (k_f + k_r) \cdot z(t) = F_z(t),$$

$$where \ F_z(t) = \frac{m_s \cdot a_y(t) \cdot h_{cg}}{t_{track}/2}$$

- $m_s \cdot \ddot{z}(t)$: Inertial force due to vertical acceleration of the sprung mass.

- $(c_f + c_r) \cdot \dot{z}(t)$: Damping force from the front and rear dampers.

- $(k_f + k_r) \cdot z(t)$: Restoring force from the front and rear springs.

- $F_z(t)$: External vertical load primarily induced by roll moment during cornering.

As the vehicle undergoes lateral acceleration in turn, the resulting roll moment is asymmetrically distributed across the left and right suspensions. This causes uneven compression, generating a net vertical force that displaces the vehicle's CG downward. The derived expression for $F_z(t)$ quantitatively captures this load transfer effect.

### 2.1.5 Lateral Dynamics Equation

The lateral dynamics equation models the vehicle's lateral motion in response to cornering forces and suspension behavior:

$$m_s \cdot \ddot{y}(t) + (c_f + c_r) \cdot \dot{y}(t) + (k_f + k_r) \cdot y(t) = m_s \cdot a_y(t)$$

- $m_s \cdot \ddot{y}(t)$: Inertial force resulting from lateral acceleration of the CG.

- $(c_f + c_r) \cdot \dot{y}(t)$: Damping force opposing lateral movement.

- $(k_f + k_r) \cdot y(t)$: Restoring force due to lateral spring displacement.

- $m_s \cdot a_y(t)$: External lateral input force from steering during cornering.

This equation helps quantify how the suspension system contributes to lateral stability and body control during aggressive directional

changes. It can also account for anti-roll bar effects depending on the modeling detail.

### 2.1.6 Yaw Rate Dynamics Equation

Yaw motion describes the vehicle's rotational behavior around the vertical axis, primarily induced by steering inputs during cornering. The yaw rate dynamics equation models the rotational response of the vehicle as follows:

$$I_z \cdot \dot{r}(t) + \left(c_f a^2 + c_r b^2\right) \cdot r(t) = M_{yaw}(t),$$

$$where \; M_{yaw}(t) \approx m_s \cdot \frac{v^2}{L} \cdot tan\,(\delta) \cdot h_{cg}$$

- $I_z \cdot \dot{r}(t)$: Yaw acceleration due to rotational inertia

- $\left(c_f a^2 + c_r b^2\right) \cdot r(t)$: Damping torque from front and rear dampers

- $M_{yaw}(t)$: External yaw moment caused by steering input

- $m_s$: Sprung mass

- $v^2/L$: Centripetal acceleration based on path curvature

- $tan\,(\delta)$: Steering angle

- $h_{cg}$ : Height of center of gravity (CG), acting as the moment arm for yaw torque

This equation captures how the vehicle reacts to steering commands, particularly during high-speed cornering where yaw stability is crucial for maintaining controllability and avoiding oversteer or understeer.

### 2.1.7 Power Spectral Density (PSD)

To quantify ride comfort in the frequency domain, Power Spectral Density (PSD) analysis is employed. It represents the distribution of acceleration energy across different frequencies and is defined as:

$$PSD(f) = \frac{|\mathcal{F}[a(t)]|^2}{T},$$

$$PSD_{weighted}(f) = PSD(f) \cdot |W(f)|^2$$

- $PSD(f)$ : Spectral representation of acceleration over time

- $W(f)$ : ISO 2631 weighting function that reflects human sensitivity to specific frequency ranges

- $PSD_{weighted}(f)$ : Frequency-weighted PSD used for comfort evaluation

This method aligns with ISO 2631 standards and enables objective evaluation of vibration-induced discomfort by considering how different frequency components affect human perception during vehicle operation.

## 2.2 Simulation – Surrogate Model Construction

To evaluate and optimize suspension design parameters effectively, a physics-based simulation model is developed using the previously derived vehicle dynamics equations. This model serves as a foundational surrogate capable of capturing key ride and handling behaviors under defined excitation conditions.

By numerically solving the pitch, roll, heave, lateral, and yaw dynamics equations, the model estimates vehicle responses such as body displacement, angular rate, and acceleration. These simulation results provide a controlled, repeatable environment to assess the effect of varying suspension parameters without the influence of experimental noise.

This simulation model plays two critical roles in the overall study. First, it offers a physically interpretable baseline for suspension tuning, helping to narrow down feasible parameter ranges before engaging in costly physical experiments. Second, it enables the construction of a simulation-based surrogate model that can be compared against experimentally derived surrogate models to verify consistency and generalizability.

As a pre-processing step to surrogate model training, Latin Hypercube Sampling (LHS) is employed to efficiently explore the parameter
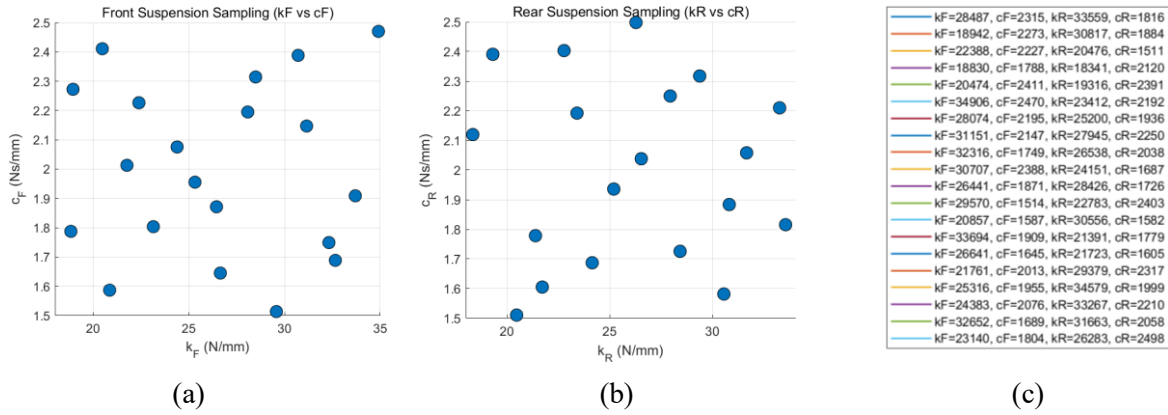
Fig. 2. (a) LHS Sample Distribution for Front Suspension Parameters ($k_f, c_f$). (b) LHS Sample Distribution for Rear Suspension Parameter ($k_r, c_r$). (c) Summary Table of 20 LHS Sample Sets for Suspension Parameters

space. This ensures a well-distributed and unbiased sample set over the multi-variable input domain, minimizing correlation between parameters.

## 2.2.1 Latin Hypercube Sampling (LHS) for Suspension Parameter Design

To ensure sufficient coverage of the multi-dimensional suspension design space while minimizing the number of required simulations, this study adopts Latin Hypercube Sampling (LHS) as a design-of-experiments (DoE) strategy. LHS is a stratified sampling technique widely used in engineering applications to efficiently distribute sample points across the input domain without redundancy.

Unlike grid sampling or purely random sampling, LHS divides each input variable's range into equally probable intervals and selects samples such that each interval is sampled exactly once. When extended to multiple variables, this method ensures a uniform and non-overlapping distribution across the parameter space. This is particularly valuable in suspension modeling, where spring stiffness and damping coefficients vary simultaneously.

Although the full suspension model originally included six parameters—front and rear spring stiffness, compression damping, and rebound damping at both axles—only four were selected for the simulation-based model:

$k_f, k_r$ and $c_f, c_r$ representing the equivalent damping.

This reduction is primarily due to the linear nature of the vehicle dynamics model, which cannot independently model the nonlinear effects of compression and rebound damping. Furthermore, reducing dimensionality improves sampling efficiency and enhances surrogate model training stability without compromising physical interpretability.

In this study, the following parameters are sampled using LHS:

- $k_f, k_r$: Front and rear spring stiffness [18–35 N/mm]

- $c_f, c_r$: Front and rear damping coefficient [1.5–2.5 Ns/mm]

A total of 20 independent sample sets were generated with 10,000 iterations of optimization to identify the best decorrelated combination. The final sample sets maintain minimal cross-correlation between variables while covering the full design domain.

The distribution of the selected samples is visualized in **Figure 2**, which illustrates the pairwise LHS sampling results for front and rear suspensions, as well as the complete list of selected sample values. Figure 2(a) shows the distribution of front spring stiffness and damping ($k_f, c_f$), while Figure 2(b) presents the corresponding distribution for the rear parameters ($k_r, c_r$). The detailed numerical

13

values of all 20 LHS sample sets are listed in Figure 2(c).

These LHS samples are then used as input conditions for the numerical dynamic model described earlier, enabling systematic simulation of suspension responses. These simulation results serve as training data for constructing the simulation-based surrogate model.

### 2.2.2 Simulation Setup and Conditions

In this section, the simulation settings, vehicle parameters, and modeling assumptions used to generate suspension response data are presented. The simulation is designed to emulate a realistic cornering maneuver along a circular trajectory, allowing evaluation of dynamic responses under longitudinal and lateral excitation.

**Vehicle Motion Profile**

The vehicle travels along a circular track with a radius of 5 meters. The driving profile is segmented into three phases:

- 0–3 seconds: Acceleration phase

- 3–7 seconds: Constant-speed cruising (3.5 m/s)

- 7–10 seconds: Deceleration to stop

This dynamic profile enables analysis of both transient and steady-state behaviors under cornering conditions.

**Initial Conditions**

- Initial pitch angle: 0 rad

- Initial pitch angular velocity: 0 rad/s

These conditions assume a steady-state equilibrium at the start of motion.

**Simulation Settings**

- Time step: 0.001 seconds

- Total simulation time: 10 seconds

- Numerical integration method: Runge-Kutta 4th/5th order (ODE45 in MATLAB)

**Modeling Assumptions**

To isolate the effect of suspension parameters, the following simplifications are applied:

- Flat and uniform road surface

- No tire slip

- Rigid body vehicle dynamics

- No aerodynamic effects

These assumptions eliminate external nonlinearities and enable clean interpretation of suspension-induced responses.

**Vehicle Parameters**

The physical properties of the simulated vehicle are summarized in **Table 1**. These include mass properties, geometric dimensions, and CG-related values required for pitch and roll calculations.

These values are applied consistently across all simulations using different LHS parameter combinations.

**Table 1. Vehicle Parameters for Dynamics Simulation**

| Parameter | Value |
|---|---|
| Sprung mass, $m_s$ | 243 kg |
| Pitch moment of inertia, $I_{yy}$ | 105 kg·m² |
| Roll moment of inertia, $I_{xx}$ | 65 kg·m² |
| Distance from CG to front axle, $a$ | 0.61 m |
| Distance from CG to rear axle, $b$ | 0.50 m |
| Half of front/rear track width, $t_f, t_r$ | 0.55 m |
| Height of CG from ground, $h_{cg}$ | 0.25 m |
| Spring stiffness, $k_f, k_r$ | 18–35 N/mm |
| Damping coefficient, $c_f, c_r$ | 1.5–2.5 Ns/mm |

### 2.2.3 Simulated Dynamic Responses

To assess the effect of suspension parameters on vehicle motion, dynamic simulations were conducted using the mathematical models

introduced earlier. Each simulation run corresponds to a unique combination of suspension parameters generated via Latin Hypercube Sampling (LHS). For each case, the time-series responses of pitch, roll, yaw rate, and lateral/heave displacements were computed under realistic driving scenarios. The following subsections present the simulation results for each motion axis in detail.

### 2.2.3.1 Pitch Dynamics Simulation Results

Based on the theoretical pitch dynamics equation presented in Section 2.1, a numerical simulation was conducted to evaluate the vehicle's pitch response under a predefined longitudinal acceleration profile. The simulation utilizes a cosine-based speed profile $v(t)$, which mimics realistic driving conditions consisting of acceleration, constant-speed cruising, and deceleration phases over a total duration of 10 seconds.

The longitudinal acceleration $a_x(t)$ was computed as the first derivative of the velocity profile, and the resulting external pitch moment $M_\theta(t)$ was obtained via the relationship:

$$M_\theta(t) = m_s \cdot a_x(t) \cdot h_{cg}$$

This moment was used as an input force to the pitch dynamics ODE, which was solved for each of the 20-suspension parameter sets generated by Latin Hypercube Sampling (LHS). The parameters included front and rear spring stiffness $(k_f, k_r)$ and damping coefficients $(c_f, c_r)$ within the predefined ranges.

**Figure 3** presents the time-domain simulation results for each sampled parameter set, including the responses of pitch angle $\theta(t)$, pitch angular velocity $\dot{\theta}(t)$, and pitch angular acceleration $\ddot{\theta}(t)$. Specifically, Figure 3(a) shows the variation in pitch angle, Figure 3(b) illustrates angular velocity, and Figure 3(c) captures angular acceleration.

Notably, increased spring stiffness tends to suppress excessive pitch angles, enhancing ride stability. Meanwhile, damping coefficients predominantly influence transient behavior, especially at the transitions between acceleration and deceleration.

The observed response diversity across different parameter combinations highlights the sensitivity of pitch dynamics to suspension configuration, reinforcing the importance of systematic optimization using surrogate models in the following sections.

### 2.2.3.2 Roll Dynamics Simulation Result

Extending the methodology applied to pitch dynamics, the roll dynamics simulation focuses on the lateral tilting behavior of the vehicle body during cornering. The vehicle follows a cosine-based velocity profile $v(t)$, as previously defined, simulating a realistic sequence of acceleration, constant-speed cornering, and deceleration phases.
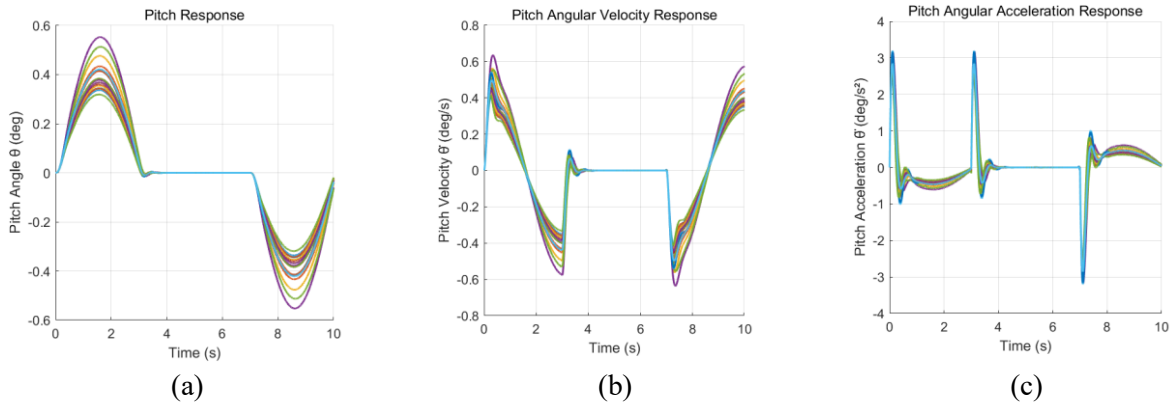


(a)     (b)     (c)

**Fig. 3. Pitch dynamics responses under varying suspension parameter sets. (a) Pitch angle $\theta(t)$ (deg). (b) Pitch angular velocity $\dot{\theta}(t)$ (deg/s). (c) Pitch angular acceleration $\ddot{\theta}(t)$ (deg/s²).**

To evaluate the lateral response, the external moment input is derived from the lateral acceleration $a_y(t)$, calculated using both centripetal and tangential components:

$$a_y(t) = \frac{v(t)^2}{R} + \frac{1}{R} \cdot \frac{dv(t)}{dt}$$

This acceleration leads to a roll moment expressed as:

$$M_\phi(t) = m_s \cdot a_y(t) \cdot h_{cg}$$

This moment is applied to the roll dynamics equation:

$$I_{xx} \cdot \ddot{\phi}(t) = M_\phi(t) - (k_f t_f^2 + k_r t_r^2) \cdot \phi(t) - (c_f t_f^2 + c_r t_r^2) \cdot \dot{\phi}(t)$$

The equation is solved across the 20-suspension parameter sets generated via Latin Hypercube Sampling (LHS), with varying values of spring stiffness and damping.

**Figure 4** presents the simulation results of roll dynamics under these varying parameter sets. Specifically, Figure 4(a) shows the roll angle $\phi(t)$, Figure 4(b) illustrates the angular velocity $\dot{\phi}(t)$, and Figure 4(c) displays the angular acceleration $\ddot{\phi}(t)$.

Compared to pitch dynamics, the roll responses exhibit sharper transients, driven by directional inertia during cornering maneuvers. These behaviors show pronounced sensitivity to damping levels and lateral stiffness distribution, underscoring their critical role in tuning vehicle handling stability.

By adhering to the same dynamic formulation and input structure as the pitch simulation, this roll simulation ensures consistency while extending the multidimensional suspension analysis framework.

### 2.2.3.3 Heave Dynamics Simulation Results

Building upon the pitch and roll dynamics analyses, the heave dynamics simulation investigates the vertical displacement response of the vehicle body under lateral loading. In cornering conditions, the roll moment generated due to lateral acceleration results in asymmetric suspension compression, which in turn induces vertical motion.

The lateral acceleration $a_y(t)$ is computed from the vehicle's velocity profile as:

$$a_y(t) = \frac{v(t)^2}{R} + \frac{1}{R} \cdot \frac{dv(t)}{dt}$$

This lateral acceleration leads to an external roll moment:

$$M_\phi(t) = m_s \cdot a_y(t) \cdot h_{cg}$$

The vertical force acting on the suspension system is then derived as:

$$F_z(t) = \frac{M_{roll}}{t_{track}/2} = \frac{m_s \cdot a_y(t) \cdot h_{cg}}{t_{track}/2}$$

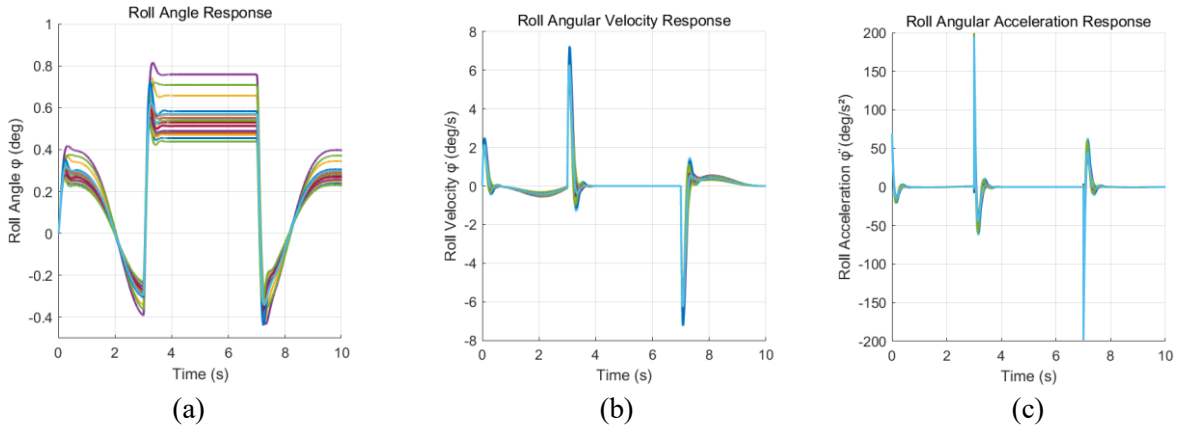This resulting vertical force is applied to the



Fig. 4. Roll dynamics responses under varying suspension parameter sets. (a) Roll angle $\phi(t)$ (deg). (b) Roll angular velocity $\dot{\phi}(t)$, (deg/s). (c) Roll angular acceleration $\ddot{\phi}(t)$ (deg/s²).
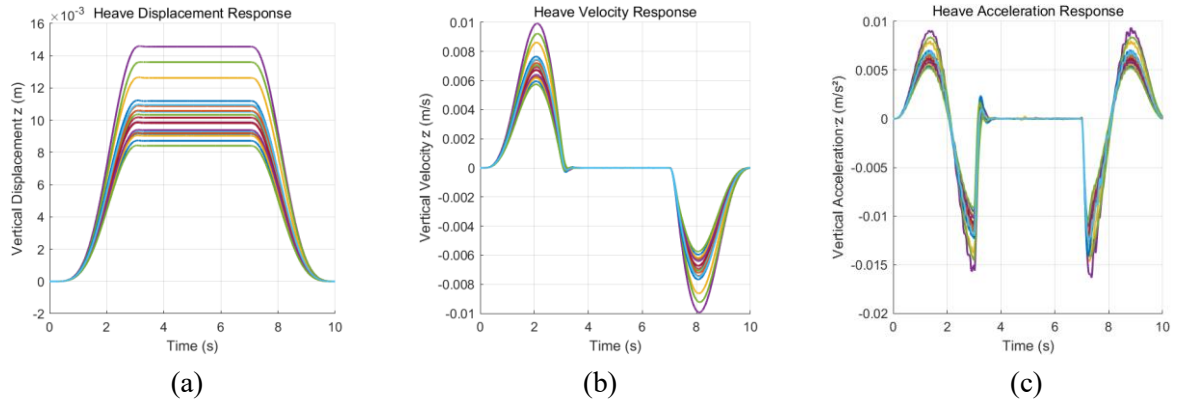
**Fig. 5. Heave dynamics responses under varying suspension parameter sets. (a) Vertical displacement $z(t)$ (m). (b) Vertical velocity $\dot{z}(t)$ (m/s). (c) Vertical acceleration $\ddot{z}(t)$ (m/s²).**

heave dynamics equation to compute the vertical response of the system.

**Figure 5** illustrates the time-domain simulation results across 20 suspension parameter sets. Specifically, Figure 5(a) shows vertical displacement $z(t)$, Figure 5(b) illustrates velocity $\dot{z}(t)$, and Figure 5(c) displays acceleration $\ddot{z}(t)$.

It is important to note that under the current simulation assumptions—specifically, a flat road with no surface irregularities—the heave response remains relatively small. In real-world conditions, heave motion would be significantly amplified by road bumps or vertical excitation inputs. Nevertheless, even the minor vertical motion captured here provides meaningful insights into the vehicle's suspension behavior during cornering.

### 2.2.3.4 Lateral Dynamics Simulation Result

The lateral dynamics simulation evaluates the vehicle's sway response under lateral acceleration. Using the same cosine-based speed profile $v(t)$, the lateral acceleration is derived as:

$$a_y(t) = \frac{v(t)^2}{R}$$

which directly yields the lateral force:

$$F_y(t) = m_s \cdot a_y(t)$$

This force acts on the vehicle's center of mass in the lateral direction, producing translational motion rather than rotational dynamics.

**Figure 6** illustrates the time-domain responses for all 20 suspension parameter sets. Specifically, Figure 6(a) shows lateral displacement $y(t)$, Figure 6(b) presents lateral velocity $\dot{y}(t)$, and Figure 6(c) shows lateral acceleration $\ddot{y}(t)$.
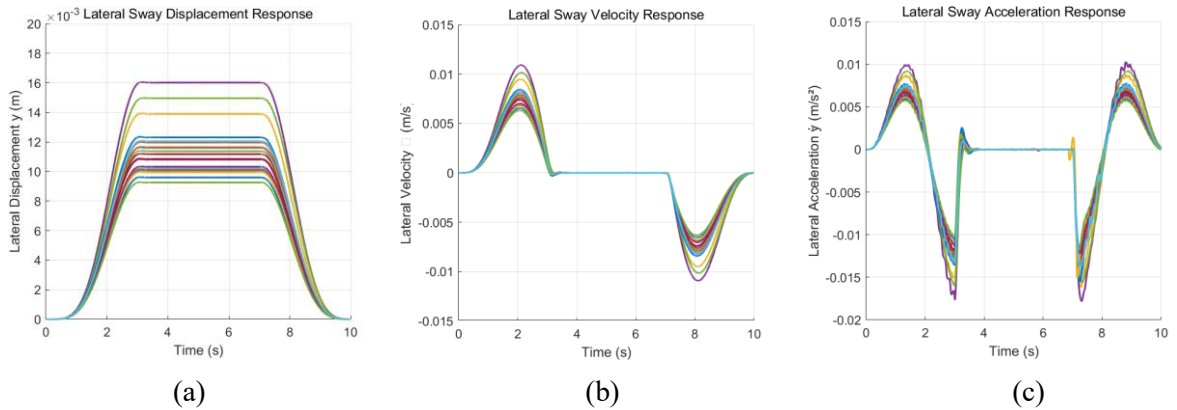


**Fig. 6. Lateral sway dynamics responses under varying suspension parameter sets. (a) Lateral displacement $y(t)$ (m). (b) Lateral velocity $\dot{y}(t)$ (m/s). (c) Lateral acceleration $\ddot{y}(t)$ (m/s²).**

Compared to roll or pitch dynamics, the magnitude of lateral sway is significantly smaller. This is primarily because the system responds to a direct force input without a moment arm such as $h_{cg}$, which amplifies motion in roll dynamics. Additionally, the simulation assumes idealized conditions including a flat road surface, no tire slip, and a rigid vehicle body—all of which inherently suppress large lateral motions.

These observations reaffirm that while lateral sway has some influence on ride comfort, its mechanical response is less pronounced than rotational dynamics under the given assumptions. Nevertheless, it remains a valuable metric for surrogate model construction.

### 2.2.3.5 Yaw Rate Dynamics Simulation Result

The yaw dynamics simulation analyzes the vehicle's rotational response about the vertical axis, which directly influences steering behavior and directional control. The governing differential equation is expressed as:

$$I_z \cdot \dot{r}(t) + (c_f a^2 + c_r b^2) \cdot r(t) = M_{yaw}(t)$$

The external yaw moment is estimated using the centripetal acceleration from circular motion:

$$M_{yaw}(t) \approx m_s \cdot \frac{v(t)^2}{L} \cdot tan(\delta) \cdot h_{cg}$$

where the steering angle $\delta$ is approximated by the known curvature $\delta \approx tan^{-1}(L/R) \approx 12.6°$. Substituting this into the governing equation

yields:

$$\dot{r}(t) = \frac{M_{yaw}(t) - (c_f a^2 + c_r b^2) \cdot r(t)}{I_z}$$

This formulation describes how suspension parameters affect yaw response dynamics.

**Figure 7** presents the yaw rate responses across 20 suspension configurations. Figure 7(a) shows the time histories of yaw rate gain $r/\delta$, while Figure 7(b) summarizes the root-mean-square (RMS) of yaw rate gain for each sample set.

The simulation results indicate that damping parameters influence both the amplitude and the settling behavior of the yaw rate. However, since the current scenario assumes ideal conditions—such as constant-radius cornering, absence of road disturbances, and perfect tire-ground contact—these dynamic responses may not fully reflect realistic behavior under aggressive or unstable driving. While increased damping seems to reduce yaw oscillations in this setup, it does not necessarily imply reduced steering responsiveness. A more comprehensive assessment under non-ideal conditions is required to evaluate such trade-offs.

### 2.2.4 Score Evaluation for Surrogate Modeling

To enable systematic surrogate modeling based on the simulation results, the dynamic responses of each suspension configuration must
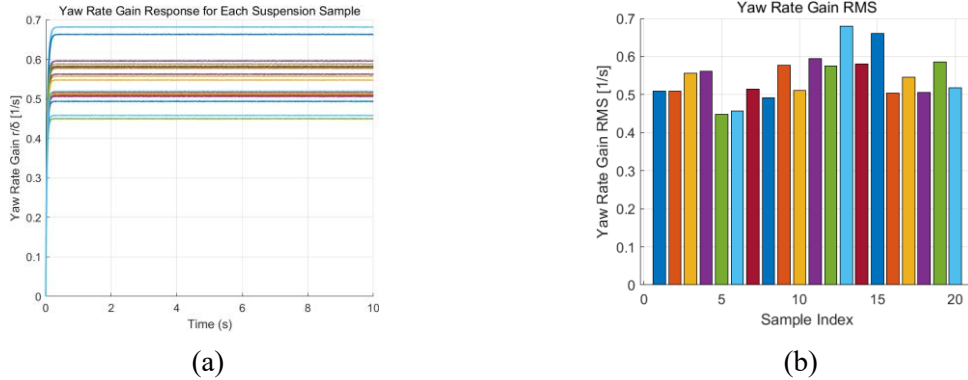


(a)



(b)

**Fig. 7. Yaw rate response under constant-radius cornering for 20 suspension parameter sets. (a) Time-domain yaw rate gain response $r/\delta$. (b) Root-mean-square (RMS) of yaw rate gain for each sample set.**

be translated into unified scalar scores. This allows for a consistent and efficient training process, regardless of the differences in physical units or scale across various performance indicators. In this section, the evaluation process is divided into two key stages: normalization of raw data and computation of weighted composite scores tailored to two design objectives, handling stability and ride comfort.

### 2.2.4.1 Data Normalization Using Min–Max Scaling

To enable effective training of the surrogate model, the simulation results must be quantitatively evaluated through unified performance scores. Since the raw outputs include physical quantities of varying units (e.g., $deg/s^2$, $m/s^2$, etc.), each metric is normalized using min–max normalization to bring all indicators onto a comparable [0, 1] scale:

$$x_{norm} = \frac{x - min(x)}{max(x) - min(x)}$$

After normalization, weighted composite scores are defined for two key performance objectives: handling stability and ride comfort. These scores are used as target outputs for Gaussian Process Regression (GPR) modeling in later steps.

### 2.2.4.2 Handling Stability Criteria and Weighting Strategy

Handling stability refers to a vehicle's capacity to maintain control and respond predictably to steering inputs, especially during dynamic maneuvers such as cornering or rapid lane changes. To evaluate this aspect systematically, three simulation-based indicators were selected:

- Yaw Rate Gain ($f_{G_{Yaw}}$): Measures the ratio of yaw rate response to steering angle input, directly quantifying steering responsiveness. A higher yaw rate gain reflects quicker, more intuitive vehicle behavior and is widely used as a benchmark for handling sharpness.
  → Assigned highest weight: $w_1 = 0.4$

- Roll Angle RMS ($f_{\phi_{Roll}}$): Indicates the vehicle body's roll motion during turns. Excessive roll can compromise stability and increase the risk of rollover, especially in high-speed maneuvers. It is a critical safety-related metric.
  → Moderate-high weight: $w_2 = 0.35$

- Lateral Acceleration RMS ($f_{a_{RMS,Lateral}}$): Represents the horizontal force experienced by the body during cornering. While not a direct indicator of control, it affects the subjective perception of agility and stability.
  → Lower weight: $w_3 = 0.25$

These weights reflect the relative importance of each metric: yaw rate gain as the most fundamental to control, followed by roll angle (linked to safety), and lateral acceleration (linked to comfort and feel). The combined handling score is expressed as:

$$f_{handling}(x) = 0.4 \cdot f_{G_{Yaw}} + 0.35 \cdot (1 - f_{\phi_{Roll}}) + 0.25 \cdot (1 - f_{a_{RMS,Lateral}})$$

The roll and lateral acceleration terms are inverted because smaller values are preferable for stability.

### 2.2.4.3 Ride Comfort Criteria and Weighting Strategy

Ride comfort assesses the degree of physical comfort experienced by passengers, focusing primarily on vibration and vertical body motion. The following indicators were selected:

- Heave Acceleration RMS ($f_{a_{RMS,Z}}$): Captures vertical vibration levels that directly influence human discomfort, especially in frequencies to which the body is sensitive. It is the most direct and physiologically relevant metric for ride quality.
  → Assigned highest weight: $w_3 = 0.45$

- Pitch Angular Acceleration RMS ($f_{a_{RMS,Pitch}}$): Reflects forward-backward tilting, which may not always be perceptible but can cause motion sickness or discomfort when persistent.
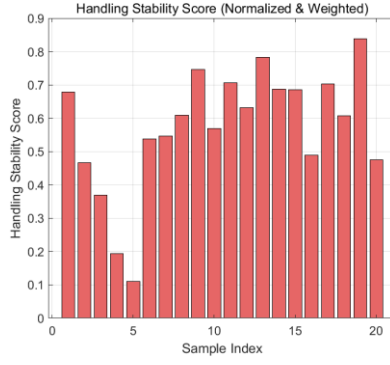
(a)
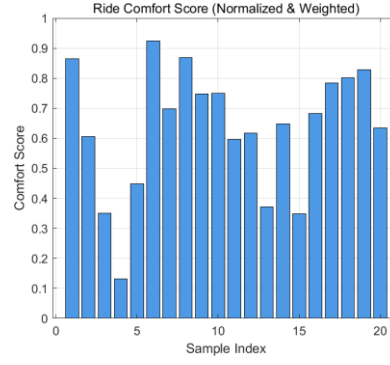


(b)

**Fig. 8. Normalized and weighted scores for each suspension parameter set (simulation-based evaluation). (a) Handling stability score. (b) Ride comfort score.**

→ Moderate weight: $w_4 = 0.30$

- Roll Angular Acceleration RMS ($f_{a_{RMS,Roll}}$): Relates to lateral body oscillation. Its contribution to comfort is less direct and often masked by seat cushioning or limited motion range.
  → Lowest weight: $w_5 = 0.25$

The comfort score is thus defined as:

$$f_{comfort}(x) = 0.45 \cdot (1 - f_{a_{RMS,Z}}) + 0.30 \cdot (1 - f_{a_{RMS,Pitch}}) + 0.25 \cdot (1 - f_{a_{RMS,Roll}})$$

A frequency-domain indicator such as Power Spectral Density (PSD) is commonly included in comfort analysis but was excluded in this study. This is because simulation assumes an idealized environment without surface irregularities or vertical input conditions under which PSD is not meaningfully defined.

**2.2.4.4 Final Note on Score Evaluation (Simulation)**

**Figure 8** presents the final normalized and weighted scores for handling stability and ride comfort across all 20 suspension parameter sets sampled via Latin Hypercube Sampling (LHS). Specifically, Figure 8(a) shows the handling stability scores, while Figure 8(b) illustrates the ride comfort scores.

These scores were computed using a weighted sum of selected performance indicators—such as yaw rate gain, roll angle, and lateral acceleration

RMS for handling, and vertical acceleration or displacement for comfort—followed by Min–Max normalization.

These results form the quantitative foundation for constructing GPR-based surrogate models in the following section, enabling efficient design optimization without repeated simulations.

**2.2.5 Pareto Optimization and User-Based Suspension Parameter Recommendation**

To identify optimal suspension parameters that balance handling stability and ride comfort, a multi-objective optimization framework based on the Pareto Front is employed. The Pareto Front comprises non-dominated solutions in which no objective (e.g., handling or comfort) can be improved without degrading the other. These solutions form the boundary of optimal trade-offs and are ideal for recommending user-specific designs based on driving preference.

The final total score is formulated as a weighted sum of the normalized handling and comfort scores:

$$f_{total}(x) = w_{handling}f_{handling}(x) + w_{comfort}f_{comfort}(x)$$

By adjusting the weight ratio $w_h : w_c$, users can prioritize either performance aspect. For instance, drivers focusing on dynamic control may prefer $w_h : w_c = 0.9 : 0.1$, while those emphasizing ride comfort may favor $0.1 : 0.9$.

**Table 2** presents the optimal suspension

parameter sets selected for each weight ratio, along with their respective handling and comfort scores.

The Pareto Front, shown in **Figure 9**, clearly illustrates the trade-off relationship between handling and comfort performance. Each colored point represents an optimal design corresponding to a specific user-defined weighting scenario, as listed in Table 2.

This optimization framework enables personalized suspension tuning that reflects the driver's intent, while remaining grounded in physics-based dynamics simulations and surrogate modeling.

As previously stated, this study adopts a weighting ratio of $w_h : w_c = 0.8 : 0.2$ to reflect the nature of Formula-style competitions, where lap time minimization and responsive cornering behavior are critical.
Although the current findings are derived solely from physics-based simulations, they offer valuable insight into the potential of surrogate-model-guided suspension design, which will be discussed further in the next section.

## 2.3 Experiment – Surrogate Model Construction

To complement the simulation-based surrogate model and evaluate its generalizability, an experimental surrogate model was constructed using real-world vibration data collected from an instrumented electric vehicle. Unlike the
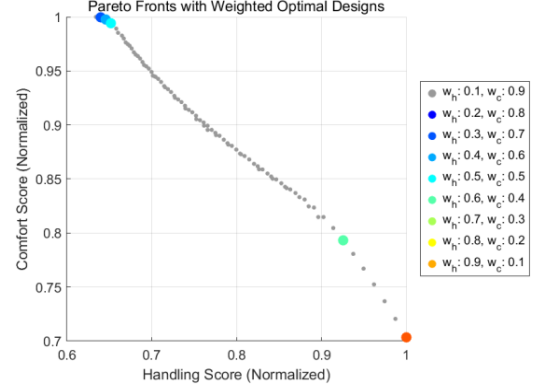


**Fig. 9. Pareto Front of handling vs. comfort performance**

simulation, which relies on simplified dynamics and idealized assumptions, the experimental model inherently captures complex nonlinearities and noise present in real-world driving environments. This allows for a more robust assessment of surrogate model performance and enhances its applicability to practical vehicle tuning tasks.

The experimental data acquisition system was designed to measure dynamic responses of the vehicle under controlled cornering scenarios. Six suspension parameters, including spring stiffness and damping coefficients for compression and rebound—were varied using Latin Hypercube Sampling (LHS) to ensure wide coverage of the design space. The corresponding dynamic responses, including roll angle, pitch angle, lateral acceleration, vertical vibration (RMS), and angular rates, were recorded using an onboard IMU sensor mounted near the vehicle's

**Table 2. Weighted optimization results (Simulation Based): Optimal scores and suspension parameters for different handling-to-comfort ratios.**

| $w_h : w_c$ | $k_{front}$ | $k_{rear}$ | $c_{front}$ | $c_{rear}$ | Handling Score | Comfort Score | Total Score |
|---|---|---|---|---|---|---|---|
| 0.1 : 0.9 | 34906.00 | 34579.00 | 2470.20 | 2030.40 | 0.64 | 1.00 | 0.96 |
| 0.2 : 0.8 | 34906.00 | 34579.00 | 2470.20 | 2030.40 | 0.64 | 1.00 | 0.93 |
| 0.3 : 0.7 | 34906.00 | 34579.00 | 2470.20 | 1978.40 | 0.65 | 1.00 | 0.89 |
| 0.4 : 0.6 | 34906.00 | 34579.00 | 2470.20 | 1926.40 | 0.65 | 0.99 | 0.86 |
| 0.5 : 0.5 | 34906.00 | 34579.00 | 1513.80 | 1822.50 | 0.93 | 0.79 | 0.86 |
| 0.6 : 0.4 | 34906.00 | 34579.00 | 1513.80 | 1510.60 | 1.00 | 0.70 | 0.88 |
| 0.7 : 0.3 | 34906.00 | 34579.00 | 1513.80 | 1510.60 | 1.00 | 0.70 | 0.91 |
| 0.8 : 0.2 | 34906.00 | 34579.00 | 1513.80 | 1510.60 | 1.00 | 0.70 | 0.94 |
| 0.9 : 0.1 | 34906.00 | 34579.00 | 1513.80 | 1510.60 | 1.00 | 0.70 | 0.97 |

center of gravity.

The following subsections detail the hardware setup, experimental procedures, and data acquisition framework employed to construct the experimental surrogate model.

### 2.3.1 Hardware Configuration and Instrumentation

A custom-built electric vehicle used for Formula SAE competitions was employed as an experimental platform. The vehicle features a lightweight tubular space frame, double wishbone suspension, and adjustable coilover shock absorbers (DNM RCP-2S), allowing controlled variation of suspension parameters.

The DNM RCP-2S shock absorber, shown in **Figure 10**, provides adjustable settings for both spring preload and damping characteristics. The preload adjustment alters the effective stiffness index $K_{eff}$, while separate knobs control compression and rebound damping at the front and rear (Figures 10b–d).

The main components of the data acquisition system include:

- Microcontroller: LOLIN D32 Pro V2.0.0 (ESP32-based) with integrated MicroSD logging and wireless capability

- Motion Sensor: SparkFun 9DoF IMU (ICM-20948), capable of capturing acceleration, angular rate, and magnetic field data at 160 Hz

- Mounting Position: IMU is mounted near the vehicle's center of gravity to minimize offset and improve motion tracking accuracy

The sampling frequency of 160 Hz was selected based on ISO 2631 guidelines, ensuring accurate capture of vertical and lateral vehicle dynamics up to ~80 Hz, which covers the dominant vibration frequencies during driving maneuvers.

### 2.3.2 Suspension Parameter Variation and Driving Protocol

To generate a comprehensive dataset of vehicle responses under diverse suspension conditions, a total of 20 suspension setups were defined using Latin Hypercube Sampling (LHS). The sampling covers six design variables: front and rear spring stiffness, compression damping, and rebound damping.

However, due to physical constraints in the experimental setup and the goal of maintaining dimensional efficiency during model training, the front and rear spring stiffnesses were unified into a single representative index $K_{eff}$. This simplification helps isolate the general trend of stiffness influence on dynamics without introducing unnecessary complexity.

The effective stiffness index ranges from 1 to 4, where the higher index represents greater spring stiffness. This mapping corresponds to the physical adjustment of preload on the DNM shock absorbers, within the actual range of 18–
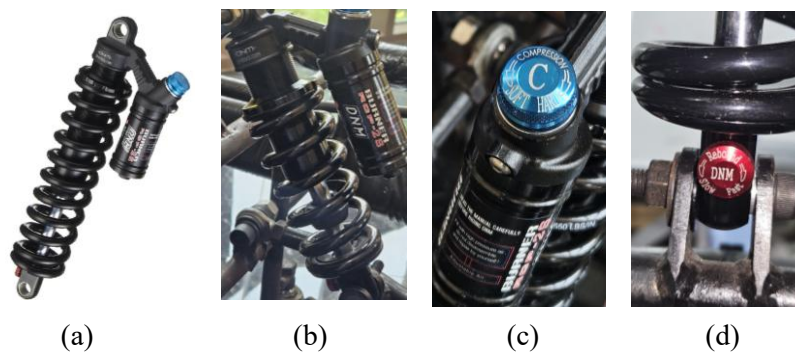


(a)  (b)  (c)  (d)

**Figure 10. DNM RCP-2S Adjustable Shock Absorber Used in the Experiment (a) Overall view of the coilover unit (b) Spring component adjusted to control stiffness (c) Compression damping knob (d) Rebound damping knob**

35 N/mm.

Similarly, each damping parameter—compression and rebound damping at front and rear—is represented using discrete index values based on physical knob levels:

- Compression damping: 1 to 12
- Rebound damping: 1 to 22

Here, higher values reflect stronger damping characteristics, roughly mapped to the damping coefficient range of 1.5–2.5 Ns/mm.

All 20 configurations were implemented on the experimental vehicle by manually adjusting the shock absorber knobs. The corresponding indexed values are summarized in **Table 3**.

Each setup was then tested under the same predefined cornering driving protocol, ensuring consistent dynamic input conditions for response comparison.

**Table 3. Suspension Parameter Index Mapping for Experimental Evaluation**

| # | $k_{eff}$ [1, 4] | $C_{COMP_{front}}$ [1, 12] | $C_{REB_{front}}$ [1, 22] | $C_{COMP_{rear}}$ [1, 12] | $C_{REB_{rear}}$ [1, 22] |
|---|---|---|---|---|---|
| 1 | 4 | 7 | 6 | 6 | 10 |
| 2 | 4 | 3 | 10 | 11 | 9 |
| 3 | 4 | 11 | 20 | 8 | 7 |
| 4 | 4 | 7 | 15 | 1 | 3 |
| 5 | 4 | 6 | 12 | 2 | 12 |
| 6 | 3 | 11 | 2 | 4 | 14 |
| 7 | 3 | 8 | 13 | 9 | 8 |
| 8 | 3 | 1 | 11 | 7 | 17 |
| 9 | 3 | 2 | 7 | 5 | 22 |
| 10 | 3 | 6 | 18 | 11 | 13 |
| 11 | 2 | 5 | 4 | 9 | 5 |
| 12 | 2 | 2 | 3 | 3 | 11 |
| 13 | 2 | 12 | 5 | 12 | 16 |
| 14 | 2 | 9 | 8 | 6 | 3 |
| 15 | 2 | 8 | 18 | 9 | 20 |
| 16 | 1 | 9 | 21 | 5 | 15 |
| 17 | 1 | 4 | 21 | 3 | 6 |
| 18 | 1 | 4 | 14 | 7 | 2 |
| 19 | 1 | 10 | 16 | 2 | 21 |
| 20 | 1 | 4 | 20 | 10 | 18 |

## 2.3.3 Experimental Dynamic Responses

To construct a surrogate model from experimental data, a set of representative response features were extracted from the vehicle's dynamic signals. These included both time-domain measures—such as RMS values—and frequency-domain indicators such as Power Spectral Density (PSD). The analysis focused on six core responses: pitch angular acceleration, roll angular acceleration, roll angle, heave acceleration, lateral acceleration, and vertical vibration PSD.

The extraction and discussion presented in this section are based on Experiment #1, corresponding to the first parameter set generated by Latin Hypercube Sampling (LHS). This configuration was selected as a representative case, reflecting high stiffness and moderate damping settings.

The detailed suspension settings of Experiment #1—including both index values and their corresponding real physical parameters—are summarized in **Table 4** below. These values were physically implemented on the test vehicle and used throughout the experimental evaluation.

The dynamic responses derived from this single configuration were used to evaluate the impact of suspension tuning on ride and handling behavior.

Since raw IMU data is affected by high-frequency noise and integration drift, appropriate filtering was required to obtain meaningful features. A 2 Hz low-pass filter was applied to most dynamic signals to suppress noise that does not reflect real vehicle motion. For angular displacements (pitch and roll angles), a complementary filter with a coefficient of 0.98 was used to blend gyroscope integration with accelerometer orientation, mitigating drift accumulation.

**Table 4. Suspension Parameter Index and Real Values for Experiment #1**

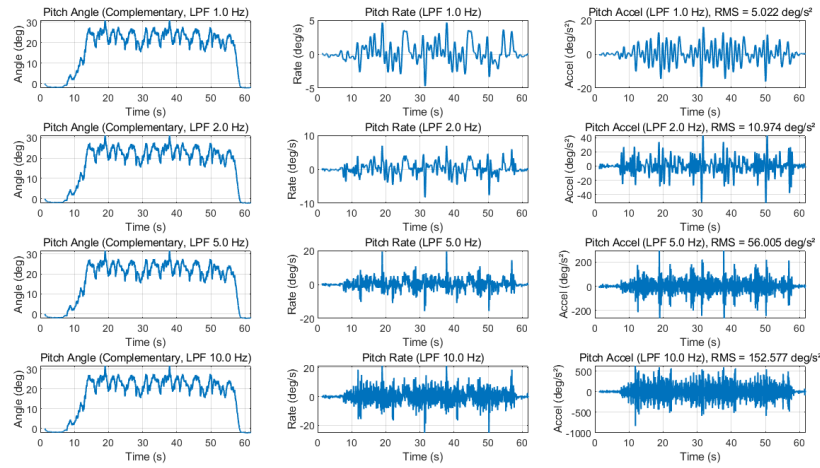| # | $K_{eff}$ | $C_{COMP_{front}}$ | $C_{REB_{front}}$ | $C_{COMP_{rear}}$ | $C_{REB_{rear}}$ |
|---|---|---|---|---|---|
| Index | 4 | 7 | 6 | 6 | 10 |
| Real Value | 35 N/mm | 2.083 Ns/mm | 1.727 Ns/mm | 2.000 Ns/mm | 1.954 Ns/mm |

**Fig. 11. Effect of Filter Cutoff Frequency on Pitch Dynamics (Experiment #1) Comparison of pitch angle (left), pitch rate (middle), and pitch angular acceleration (right) for cutoff frequencies of 1, 2, 5, and 10 Hz.**

Although the filter cutoff frequency was not formally optimized, the chosen values were selected through empirical testing to balance noise suppression and dynamic fidelity. For each of the six responses, RMS values were computed after filtering to quantify motion intensity. Notably, the PSD was not used for simulation-based modeling, but in this experimental context, it provides valuable information on how design parameters affect the spectral content of vertical vibrations and may serve as an informative feature for future surrogate modeling.

### 2.3.3.1 Pitch Angular Acceleration RMS

While pitch angular acceleration is often considered a basic indicator of longitudinal body motion, its relevance in this experiment is limited compared to roll-based metrics. The RMS of pitch angular acceleration was calculated after applying a 2 Hz low-pass filter, resulting in a value of 10.97 deg/s², which is within the expected range for aggressive electric vehicle maneuvers.

**Figure 11** illustrates how different filter cutoff frequencies affect the measured pitch angle, rate, and acceleration signals from Experiment #1 (as defined in Table 4). While the higher cutoff values capture more transient motion, they also introduce amplified sensor noise, particularly in the acceleration channel.

Although pitch motion contributes to ride comfort, it played a relatively minor role in our test scenario, where lateral dynamics dominated due to the tight turning layout. As such, pitch response is included primarily to complete the characterization of vehicle motion.

### 2.3.3.2 Roll Angular Acceleration RMS

Roll angular acceleration serves as a more dominant measure of dynamic response in this experiment, reflecting the severity of lateral body motion during sharp cornering maneuvers. After applying a 2 Hz low-pass filter (LPF), the RMS value of roll angular acceleration was 49.49 deg/s², indicating the magnitude of lateral disturbance perceived by the driver.

This metric is particularly valuable for evaluating handling stability, as rapid angular shifts around the roll axis are often associated with reduced driver confidence or potential loss of control. Therefore, roll angular acceleration is considered a primary indicator of ride quality in this context.

**Figure 12** visualizes the roll angle, angular velocity, and angular acceleration responses under various cutoff frequencies (1, 2, 5, and 10 Hz) for Experiment #1, as defined in Table 4. As the filter frequency increases, high-frequency oscillations become more pronounced, and the
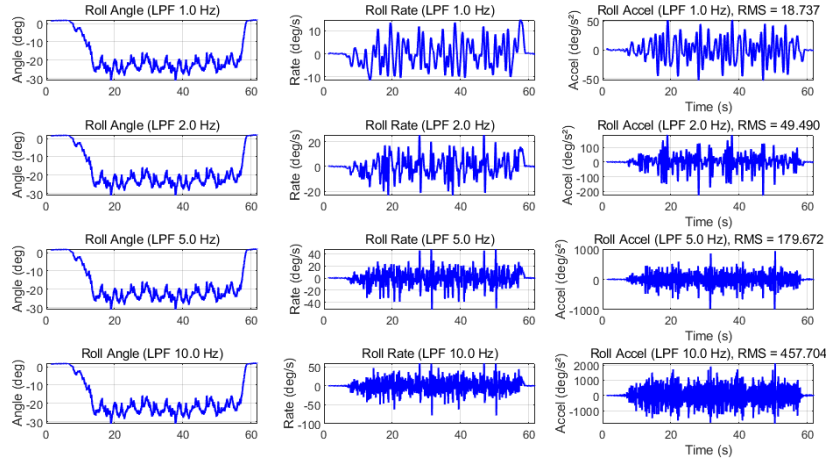
**Fig. 12. Effect of Filter Cutoff Frequency on Roll Dynamics (Experiment #1) Comparison of roll angle (left), roll rate (middle), and roll angular acceleration (right) for cutoff frequencies of 1, 2, 5, and 10 Hz.**

RMS value increases significantly highlighting the trade-off between signal fidelity and noise suppression.

### 2.3.3.3 Roll Angle RMS

The roll angle is arguably the most critical indicator of vehicle stability during cornering in this study. As illustrated in **Figure 12**, experimental observations confirmed that when the effective stiffness $K_{eff}$ f was reduced, the vehicle exhibited pronounced body lean, which was felt distinctly by the driver. The RMS value for roll angle exceeded 20 degrees, indicating a significant degree of roll during cornering.

However, this high value may be partially attributed to surface irregularities and IMU drift or sensor resolution limits, as the test environment included minor slopes and uneven pavement. Nonetheless, roll angle remains the most reliable indicator of lateral stability and vehicle posture under load transfer.

### 2.3.3.4 Heave Acceleration RMS

Heave acceleration RMS is a key metric for evaluating ride comfort. In this test environment, the presence of small rocks and uneven terrain introduced uncontrolled vertical inputs. As shown in **Figure 13**, the RMS value after applying a 1 Hz low-pass filter was 31.73 m/s²,
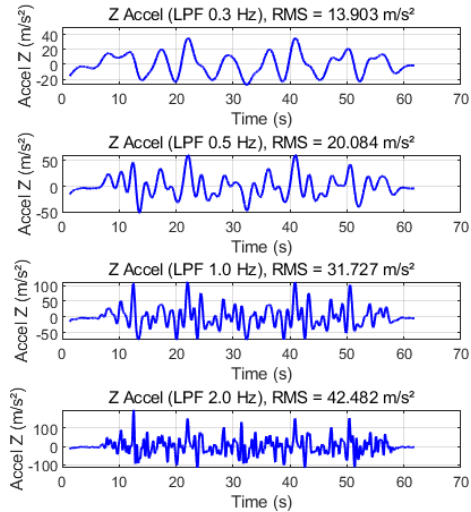


**Fig. 13. Heave Acceleration Time-Series and RMS under Varying LPF Cutoffs**

indicating a relatively high level of vertical excitation.

Although the noise floor may include non-representative spikes due to terrain irregularity, the heave response remains critical, as it directly relates to passenger comfort and body control in real-world conditions.

### 2.3.3.5 Lateral Acceleration RMS

Lateral acceleration RMS serves as a core indicator of vehicle handling dynamics, particularly in high-load cornering scenarios. In this study, the vehicle platform corresponds to a

25

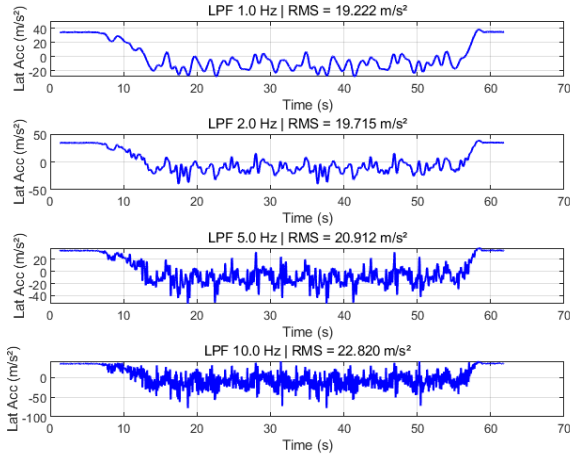**Fig. 14. Lateral Acceleration RMS Analysis with LPF Variations**

student-designed formula-style race car, which, although not a commercial sports car, exhibits significant lateral acceleration characteristics due to its lightweight and low center of gravity.

As shown in **Figure 14**, the RMS values of lateral acceleration were computed after applying various low-pass filter (LPF) cutoff frequencies. With a 2 Hz filter, the RMS value reached 19.72 m/s², which aligns with expected levels for compact, high-agility racing vehicles during aggressive cornering.

This highlights the importance of lateral dynamics in the subjective and objective evaluation of maneuverability. Although yaw rate gain could not be measured due to sensor and steering limitations, lateral acceleration remains a key variable in surrogate modeling, capturing both driver experience and the vehicle's dynamic envelope.

**2.3.3.6 Heave Acceleration PSD**

The Power Spectral Density (PSD) of the heave acceleration signal was analyzed to understand how vertical vibration energy is distributed across different frequency bands for each test configuration. As shown in **Figure 15**, the experimental PSD is relatively broad and flat across the 0.5–50 Hz range, with dominant peaks around 50 dB(m²/s⁴/Hz).

Such a spread in spectral energy likely results from surface irregularities and broadband vertical
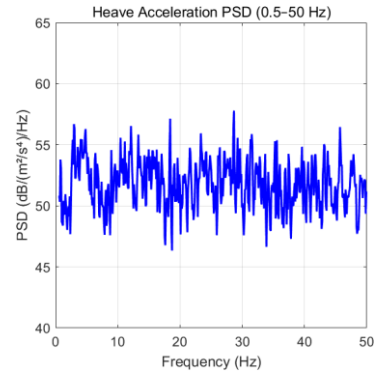


**Fig. 15. Power Spectral Density of Heave Acceleration (0.5–50 Hz)**

excitation encountered in the real-world test environment. Importantly, while PSD was not utilized in simulation-based modeling, its inclusion here provides insight into how suspension parameter variations influence the spectral content of vertical ride disturbances.

Therefore, the PSD analysis offers an important reference point for evaluating and comparing the dynamic performance of different suspension settings under experimental conditions.

**2.3.4 Score Evaluation for Experimental Surrogate Modeling**

To enable surrogate modeling based on experimentally measured vehicle responses, each dynamic indicator must be translated into a normalized scalar score. These scores are used to train data-driven surrogate models that map suspension settings to handling and comfort performance. Similar to the simulation framework, this section outlines the data normalization process and the formulation of composite scores using weighted indicators

**2.3.4.1 Data Normalization Using Min–Max Scaling**

As the measured response values—such as angular acceleration and vibration levels—have varying physical units and ranges, they are normalized to a common scale [0, 1] using min–max normalization:

$$x_{norm} = \frac{x - min(x)}{max(x) - min(x)}$$

To ensure interpretability and consistent optimization direction, the normalized indicators are inverted using $1 - f(x_{norm})$, since lower values of vibration and acceleration are generally preferable for both ride comfort and stability.

### 2.3.4.2 Handling Stability Criteria and Weighting Strategy (Experimental)

Handling stability refers to the vehicle's ability to maintain lateral balance and respond accurately to steering inputs during cornering. In this experimental context, yaw rate gain was not available due to limitations in steering angle input measurement. Instead, two alternative indicators were adopted:

- Roll Angle RMS ($f_{\phi_{Roll}}$): Reflects the degree of body tilting during turns. A higher roll angle indicates reduced lateral stability and a greater risk of vehicle turnover or reduced driver confidence.
  → Assigned weight: $w_1 = 0.5$

- Lateral Acceleration RMS ($f_{a_{RMS,Lateral}}$): Captures the side-force acting on the vehicle body during cornering. While this does not directly indicate stability, it reflects the sharpness of the maneuver and contributes to the sensation of agility.
  → Assigned weight: $w_2 = 0.5$

These indicators were selected for their physical relevance and direct observability via onboard IMU sensors. Equal weighting was applied to ensure balanced evaluation of both body control and maneuver responsiveness.

The final handling score was computed as:

$$f_{handling}(x) = 0.5 \cdot (1 - f_{\phi_{Roll}}) + 0.5 \cdot (1 - f_{a_{RMS,Lateral}})$$

where all terms are min–max normalized and inverted to reflect the desirability of lower values.

### 2.3.4.3 Ride Comfort Criteria and Weighting Strategy (Experimental)

Ride comfort evaluates the vehicle's vibration isolation performance, which strongly affects passenger perception and physical fatigue. In this experiment, four response features were used:

- Heave Acceleration RMS ( $f_{a_{RMS,Z}}$ ): Quantifies vertical vibration of the vehicle body and is the most representative metric of ride discomfort.
  → Assigned highest weight: $w_3 = 0.4$

- Pitch Angular Acceleration RMS ($f_{a_{RMS,Pitch}}$): Represents fore-aft body motion, which may contribute to motion sickness or discomfort during acceleration and braking.
  → Assigned weight: $w_4 = 0.2$

- Roll Angular Acceleration RMS ($f_{a_{RMS,Roll}}$): Indicates lateral body oscillation, which can be uncomfortable especially during repeated cornering.
  → Assigned weight: $w_5 = 0.2$

- Heave PSD ($f_{PSD}$): Captures the frequency distribution of vertical vibrations. Higher energy content in the 0–20 Hz range (human sensitivity) correlates with discomfort.
  → Assigned weight: $w_6 = 0.2$

The final comfort score is calculated as:

$$f_{comfort}(x) = 0.4 \cdot (1 - f_{a_{RMS,Z}}) + 0.2 \cdot (1 - f_{a_{RMS,Pitch}}) + 0.2 \cdot (1 - f_{a_{RMS,Roll}}) + 0.2 \cdot (1 - f_{PSD})$$

Each feature is normalized via min–max scaling. The inclusion of PSD differentiates this experimental study from the simulation, reflecting the real-world influence of uneven surfaces

### 2.3.4.4 Final Note on Score Evaluation (Experimental)

**Figure 16** presents the normalized and weighted scores for all 20 experimental
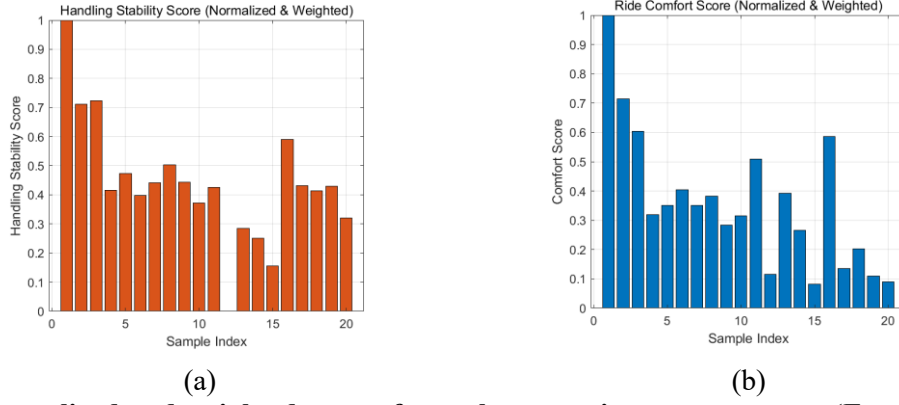
**Fig. 16. Normalized and weighted scores for each suspension parameter set (Experiment-based evaluation). (a) Handling stability score. (b) Ride comfort score.**

suspension configurations. Figure 16(a) shows the handling stability scores based on roll angle and lateral acceleration, while Figure 16(b) displays the ride comfort scores derived from vertical and angular vibration responses, including heave acceleration and pitch/roll angular acceleration.

Unlike the simulation analysis, this experimental evaluation includes Power Spectral Density (PSD) as part of the comfort metric. Given that real-world roads introduce broadband vibrations, PSD plays a crucial role in capturing discomfort associated with specific frequency bands.

These experimentally obtained scores serve as the basis for constructing GPR surrogate models that reflect actual driving responses, enabling data-driven optimization tailored to real-world suspension performance.

### 2.3.5 Pareto Optimization and User-Based Suspension Parameter Recommendation

The experimental scores derived from the surrogate models were also subjected to Pareto-based multi-objective optimization, following a similar structure as described in the simulation analysis (see Section 2.2.5). While the score formulation and weighting strategy remain consistent, the practical utility of experimental data lies in its ability to reflect real-world driving conditions, including surface irregularities and sensor noise—factors absent in the simulation.

As before, the total score was computed as a weighted sum of the normalized handling and comfort scores:

$$f_{total}(x) = w_{handling} f_{handling}(x) + w_{comfort} f_{comfort}(x)$$

**Table 5** presents the optimal suspension settings under varying handling–comfort priorities. Unlike in simulation, the experimental data

**Table 5. Weighted optimization results (Experiment Based): Optimal scores and suspension parameters for different handling-to-comfort ratios.**

| $w_h : w_c$ | $K_{eff}$ | $C_{COMP_{front}}$ | $C_{REB_{front}}$ | $C_{COMP_{rear}}$ | $C_{REB_{rear}}$ | Handling Score | Comfort Score | Total Score |
|---|---|---|---|---|---|---|---|---|
| 0.1 : 0.9 | 3.9977 | 6.9874 | 4.5080 | 6.8938 | 9.8641 | 1.0406 | 0.9560 | 1.0321 |
| 0.2 : 0.8 | 3.9986 | 6.1913 | 5.9283 | 7.1249 | 10.397 | 1.0347 | 0.9839 | 1.0245 |
| 0.3 : 0.7 | 3.9987 | 8.4127 | 5.5820 | 6.7828 | 9.6761 | 1.0354 | 0.9983 | 1.0242 |
| 0.4 : 0.6 | 3.9973 | 10.010 | 5.5346 | 7.0658 | 9.7118 | 1.0363 | 0.9976 | 1.0208 |
| 0.5 : 0.5 | 3.9973 | 4.9636 | 6.4233 | 7.0811 | 9.9010 | 1.0302 | 0.9970 | 1.0136 |
| 0.6 : 0.4 | 3.9983 | 3.7322 | 5.7721 | 7.7535 | 9.8233 | 1.0194 | 1.0014 | 1.0086 |
| 0.7 : 0.3 | 3.9957 | 3.7152 | 6.6068 | 6.8656 | 9.8009 | 1.0257 | 0.9937 | 1.0033 |
| 0.8 : 0.2 | 3.9987 | 6.3360 | 5.8501 | 6.5610 | 9.7477 | 1.0285 | 1.0021 | 1.0074 |
| 0.9 : 0.1 | 3.9965 | 3.7035 | 6.0992 | 7.6429 | 9.7489 | 1.0201 | 1.0022 | 1.0040 |

revealed a notably consistent trend: higher spring stiffness $(K_{eff})$ values tend to yield high scores in both handling and comfort. This suggests that, within the tested configuration space, increased stiffness improved cornering stability without significantly degrading ride quality. This finding will be discussed in more detail in the results section (Section 3.3).

This empirical optimization confirms that the score-based evaluation system, when applied to real data, can still effectively guide user-specific suspension tuning. The inclusion of physically measured dynamics adds confidence to the predictive capabilities of the surrogate model and validates the usefulness of the proposed approach beyond simulation environments.

# 3. Results and Discussion

## 3.1 Pareto Front Analysis

This section provides a comparative analysis of the Pareto fronts derived from both simulation-based and experiment-based surrogate models. While multi-objective optimization was already introduced as a key tool for balancing handling stability and ride comfort, here we focus on how the trade-off manifests across actual data-driven and physics-based models.

Each Pareto front illustrates the optimal trade-off boundary beyond which no performance metric can be improved without sacrificing the other. By comparing the shapes and trends of the two fronts, insights are drawn about consistency, robustness, and practical applicability of the design space. Notably, certain suspension configurations, especially those with higher spring stiffness, demonstrate consistent performance regardless of the weighting ratio. This suggests their suitability as a baseline or universal setup across a variety of user preferences.

### 3.1.1 Simulation-Based Pareto Front

As shown in **Table 2**, the spring stiffness values $k_f = 34906\,N/m$ and $k_r = 34579\,N/m$ remain fixed at their upper bounds across all optimal configurations. This consistent selection—regardless of the handling-to-comfort weight ratio—suggests that maximizing spring stiffness benefits both ride comfort and handling stability in the simulation environment. Hence, it can be considered a robust baseline design element.

In contrast, the damping coefficients $c_f$ and $c_r$ vary noticeably across the Pareto front. As illustrated in **Figure 17**, configurations emphasizing ride comfort (left side of the curve) tend to adopt higher damping values, while those prioritizing agile handling (right side) favor lower damping. Although this may appear counterintuitive—given that higher damping is often associated with greater control—it reflects the characteristics of the simulation model.
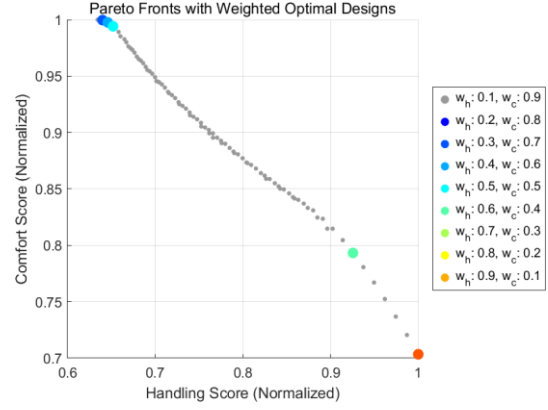


**Fig. 17. Simulation-based Pareto front with optimal designs for each weight ratio $w_h : w_c$.**

The model is based on a second-order ordinary differential equation (ODE) assuming idealized road conditions with no high-frequency disturbances. Under such assumptions, excessive damping can suppress dynamic responsiveness, thereby negatively affecting handling performance. Consequently, the observed trend in damping variation is a rational outcome of the model's simplifications.

Overall, **Figure 17** shows that while spring stiffness should be maximized by default, damping parameters require tailored tuning based on the user's performance goals and expected road conditions.

### 3.1.2 Experimented-Based Pareto Front

In the experiment-based Pareto front shown in **Table 5** and **Figure 18**, a consistent trend is observed: the optimal spring stiffness values remain at their upper limits ($k \approx 3.9987$) regardless of the handling-comfort weight ratio. This mirrors the simulation findings and reinforces the conclusion that stiffer suspension settings are beneficial for both handling and comfort, even under real-world measurement conditions.

However, in contrast to the simulation results, the damping coefficients in the experiment do not exhibit a clear or systematic trend along the trade-off curve. While minor fluctuations are present, the magnitude of variation is small and does not correlate meaningfully with the weight distribution. This suggests that damping played a
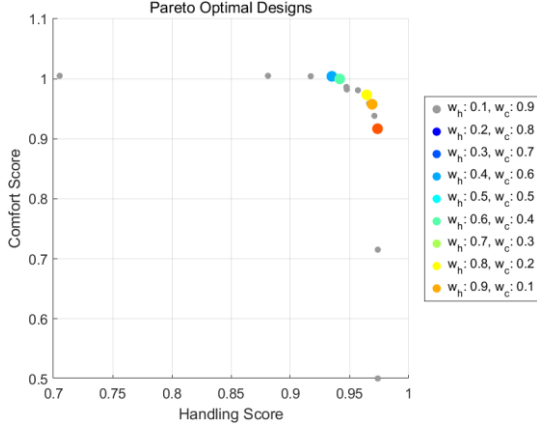
**Fig. 18. Experiment-based Pareto front with optimal designs for each weight ratio $w_h$: $w_c$.**

less significant role in experimental evaluations, possibly due to external noise or limitations in measurement resolution.

Moreover, unlike the nearly linear Pareto front obtained from simulation-based models, the experimental Pareto front in **Figure 18** exhibits a more visibly curved structure. This curvature indicates that performance trade-offs between handling and comfort are more nuanced in real-world conditions. Instead of a uniform linear trade-off, the curved shape implies that certain configurations, especially those with high spring stiffness, can provide balanced performance across various weighting preferences. This nonlinearity reflects physical effects and variabilities not captured in the deterministic simulation, highlighting the richer behavior of actual dynamic systems.

The limited impact of damping observed on the experimental front will be explored further in Section 3.3, where surrogate model generalization and uncertainty are discussed. This finding underscores the importance of validating simulation-based predictions through physical measurements to detect potential discrepancies in parameter sensitivity.

## 3.2 Performance Comparison at Target Ratio ($w_h$: $w_c = 0.8$: $0.2$)

To quantitatively assess the effectiveness of the surrogate-based optimization, performance at the target weighting ratio ($w_h$: $w_c = 0.8$: $0.2$)—

**Table 6. Suspension Parameter Changes After Optimization ($w_h$: $w_c$=0.8:0.2)**

| Parameter | Initial Value | Optimal Value |
|---|---|---|
| $K_{front}$ [N/m] | 26500 | 34906 |
| $K_{rear}$ [N/m] | 26500 | 34579 |
| $C_{front}$ [Ns/m] | 2000 | 1514 |
| $C_{rear}$ [Ns/m] | 2000 | 1511 |

**Table 7. Score Improvement from Initial to Optimal Configuration**

| Score Type | Initial Score | Optimal Score | Improvement Rate |
|---|---|---|---|
| Handling | 0.552 | 1.000 | +81% |
| Comfort | 0.654 | 0.688 | +5% |
| Total Score | 0.572 | 0.938 | +64% |

selected to reflect Formula-style high-speed cornering scenarios—was analyzed using simulation data.

As shown in **Table 6**, the initial values for each suspension parameter were set at the midpoints of their respective constraint ranges. The optimal configuration discovered via Pareto-guided search significantly increased the front and rear spring stiffnesses (from 26,500 N/m to 34,906 N/m and 34,579 N/m), while moderately reducing damping values (from 2,000 Ns/m to approximately 1,511–1,514 Ns/m). This outcome reinforces the earlier observation in Section 3.1.1 that stiffer springs consistently enhance handling performance, while lower damping—though counterintuitive—is beneficial under the idealized simulation conditions assumed in the model.

**Table 7** summarizes the resulting performance improvement. The handling score reached its maximum (from 0.552 to 1.000, an 81% increase), while comfort was only slightly affected (a 5% improvement from 0.654 to 0.688), resulting in an overall total score improvement of +64%.

These findings suggest that the optimized suspension setting not only meets the dynamic requirements of high-speed maneuvering but also maintains acceptable ride quality. Thele experimental validation is not included here due

31

to issues discussed later in Section 3.3, namely overconfidence, underestimated uncertainty, and overestimated performance, this simulation-based result clearly demonstrates the potential for significant real-world benefits, such as reduced lap times and improved cornering stability, when the proposed configuration is implemented on track.

### 3.3 Surrogate Model Assessment

This section evaluates the reliability and limitations of the surrogate models constructed from both simulation and experimental data. While the models successfully captured key trends in score responses and provided a useful basis for optimization, several caveats must be considered—particularly in the experimental case.

**Strengths:**
The surrogate models, particularly those trained on simulation data, demonstrated strong monotonicity and consistency. They successfully reflected known physical relationships, such as the positive contribution of increased spring stiffness to handling and comfort metrics. Furthermore, the Pareto-optimal trends derived from these models aligned well with the expected behavior under deterministic dynamics, validating their utility for preliminary design exploration.

**Limitations in Experimental Models:**
However, when applied to experimental data, the surrogate models exhibited signs of overconfidence—overfitting the limited sample space while underestimating inherent uncertainty. For instance, the damping coefficients, which showed clear influence in simulation-based predictions, displayed low sensitivity in experimental evaluations. This may stem from:

- A limited number of physical data samples,

- Measurement noise or resolution limits,

- Inadequate signal filtering,

- And the inherent variability in real-world vibration data.

As a result, the experimental comfort scores tended to be more compressed and less differentiated across configurations, making it difficult to clearly detect the effects of certain parameters.

### 3.4 Discussion and Future Work

This study presents a structured approach to suspension optimization using surrogate modeling and Pareto-based multi-objective analysis. Through both simulation- and experiment-based frameworks, it was shown that data-driven score metrics can successfully guide performance-driven parameter selection, particularly regarding spring stiffness and its consistent role in enhancing both handling and comfort.

However, several limitations must be addressed to improve the fidelity and real-world applicability of the proposed methodology.

**Need for More Precise and Repetitive Data:**
To increase the robustness of experiment-based surrogate models, it is essential to improve the precision and consistency of the collected data. This includes conducting multiple repeated test runs under controlled conditions to reduce variability and enable better statistical confidence in model training.

**Sensor Calibration and Signal Processing Improvements:**
Future experiments should include proper calibration of the IMU sensor and revisiting the cutoff frequency used in low-pass filtering (LPF). Fine-tuning this parameter may allow for better preservation of informative vibration signals. In addition, incorporating auxiliary sensors—such as wheel accelerometers or load cells—may provide complementary data for better capturing dynamics.

**Advanced Modeling and Optimization Techniques:**
Beyond Gaussian Process Regression (GPR), advanced techniques such as Bayesian Optimization, Monte Carlo-based Uncertainty Quantification, or Physics-informed Neural Networks (PINNs) could be explored to enhance

model generalization and provide better reliability in noisy environments.

**Real-World Application Potential:**
Most importantly, this research highlights the feasibility of transitioning from data-driven experimental surrogate modeling to actual vehicle setup recommendations. By refining the model inputs and reducing experimental uncertainty, the methodology may be extended toward practical suspension tuning in racing or performance vehicle applications.

# 4. Conclusion

This study addressed the suspension parameter optimization problem with the goal of minimizing lap time, particularly focusing on the trade-off between handling and ride comfort in high-speed cornering. By setting a target weighting ratio of 0.8 (handling) to 0.2 (comfort), we interpreted the design implications from a vehicle dynamics perspective and validated our findings through both simulation-based modeling and experimental testing.

The proposed approach revealed that maximizing spring stiffness consistently contributes to performance in both handling and comfort, while damping requires more adaptive tuning depending on the assumed driving conditions. Surrogate models built using Gaussian Process Regression enabled Pareto-guided optimization within a constrained design space.

As summarized in **Table 7**, the resulting performance improvement was substantial:

- The handling score increased from 0.552 to 1.000, an 81% improvement,

- The comfort score improved slightly from 0.654 to 0.688 (+5%),

- And the overall total score increased by +64%.

These results clearly demonstrate the effectiveness of surrogate-based optimization in enhancing cornering stability while preserving acceptable ride comfort.

Experimental validation further supported the practical applicability of the method, while also revealing limitations such as model overconfidence and underestimated uncertainty. Despite these challenges, the framework presents a viable foundation for real-world suspension tuning. Future work may incorporate techniques like Bayesian Optimization and Uncertainty Quantification to further refine performance predictions and reduce reliability gaps.

Ultimately, this research confirms the potential of data-driven surrogate modeling as a robust tool for dynamic vehicle setup in performance-focused applications.

# 5. Reference

[1] Kim, H. T., Kim, J. W., Cho, J. G., Koo, J. S., Kang, S., & Jeong, R. (2016). A study on suspension optimization of the Korean Personal Rapid Transit Vehicle. *Transactions of the Korean Society of Mechanical Engineers A*, 40(3), 317–326. https://doi.org/10.3795/ksme-a.2016.40.3.317

[2] Dzakaria, A., S. Mansor, & S.A.A Bakar. (2021). Feasibility Study of surrogate model for the application of Vehicle Suspension System. *Journal of Transport System Engineering*, 15–28. https://doi.org/10.11113/jtse.v8.170

[3] Xue, H., Gobbi, M., & Matta, A. (2023). Multi-fidelity surrogate-based optimal design of Road Vehicle Suspension Systems. *Optimization and Engineering*, *24*(4), 2773–2794. https://doi.org/10.1007/s11081-023-09793-0

[4] Tao, S., Shintani, K., Bostanabad, R., Chan, Y.-C., Yang, G., Meingast, H., & Chen, W. (2017). Enhanced gaussian process metamodeling and collaborative optimization for vehicle suspension design optimization. *Volume 2B: 43rd Design Automation Conference*. https://doi.org/10.1115/detc2017-67976

[5] Mitra, A. C., Soni, T., Kiranchand, G. R., Khan, S., & Banerjee, N. (2015). Experimental design and optimization of vehicle suspension system. *Materials Today: Proceedings*, *2*(4–5), 2453–2462. https://doi.org/10.1016/j.matpr.2015.07.186

[6] Thomas, S. S., Palandri, J., Lakehal-Ayat, M., Chakravarty, P., Wolf-Monheim, F., & Blaschko, M. B. (2023). Kinematics design of a Macpherson suspension architecture based on Bayesian optimization. *IEEE Transactions on Cybernetics*, *53*(4), 2261–2274. https://doi.org/10.1109/tcyb.2021.3114403

[7] 김재훈, & 정도연. (2018). 서스펜션 K&C 및 쇽업소버 최적화 기법 연구. *한국자동차공학회 춘계학술대회*, 422-423.

[8] 정준영, 유정주, 변경석, & 조현규. (2024). 자동차 브레이크 패드 마모량 측정센서 브라켓의 다이나믹크리깅 대리모델 기반 설계최적화. *한국전산구조공학회논문집 제37권 제2호*, 95-101.

[9] 홍성욱, 김재은, 김재용, & 장강원. (2015). 차량 서스펜션의 근사 모델 기반 다목적 최적화 비교 연구. *대한기계학회 춘추학술대회*, 2706-2708.

# 주행목적 기반 서스펜션 파라미터 최적화를 위한 대리모델 개발 연구

한동준 [1†] · 양지우 [1] · 김영근 [1*]

[1] 한동대학교 기계제어공학부

# Surrogate Models for Optimizing Suspension Parameters Based on Driving Purpose

Dongjun Han[1†], Jiwoo Yang[1], Youngkeun Kim[1*]

[1]School of Mechanical and Control Engineering, Handong Global University

**Abstract:** This study replaces the iterative optimization process through experimentation with a data-driven surrogate model to derive the optimal suspension parameter values more quickly and efficiently based on the user's driving objectives. In this research, Gaussian Process Regression (GPR) is employed to create the model. The trade-off relationship between driving stability and ride comfort is analyzed, and the Pareto optimal set is derived. Subsequently, the Weighted Sum Method is applied to assign weights between Handling stability and ride comfort based on the user's preferred suspension performance. Through this approach, optimal suspension parameters (spring, compression damper, rebound damper) values were provided. The results demonstrated that, compared to the initial design, the optimized suspension design enhanced either ride comfort or handling Stability according to the user's driving goals.
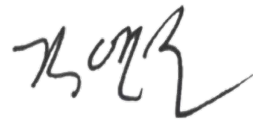
**초록:** 차량의 우수한 승차감과 핸들링 성능을 구현하기 위해서는 쇽업소버의 역할이 매우 중요하다. 그러나 쇽업소버 튜닝의 경우, 차량의 목표 성능을 만족시키기 위해 엔지니어들의 경험적 지식에 의존하며 수많은 시행착오를 거쳐 이루어진다. 본 연구는 실험을 통한 반복적인 최적값 도출 방식을 대신하여, 데이터 기반 대리모델을 활용해 사용자의 주행 목적에 따른 최적의 서스펜션 파라미터 값을 더 빠르고 효율적으로 도출한다. 본 연구에서는 모델 생성을 위해 가우시안 과정 회귀를 활용한다. 또한, 주행안정성과 승차감 간의 트레이드오프 관계를 분석하고, 이를 바탕으로 파레토 최적해 집합을 도출한다. 이후, 사용자가 선호하는 서스펜션 성능에 따라 주행 안정성과 승차감 간에 가중치를 부여하는 가중치 합 방법을 적용한다. 이를 통해 최적의 서스펜션 파라미터(스프링, 컴프레션 댐퍼, 리바운드 댐퍼) 값을 제시할 수 있었다. 생성된 대리모델의 성능을 확인하기 위해, 시뮬레이션과 실험을 통해 비교 분석하였고, 초기 설계와 비교한 결과, 최적화된 서스펜션 설계를 통해 사용자의 주행 목적에 따른 승차감 또는 핸들링 성능의 향상을 확보할 수 있었다.

Reference

(1) Kim, H. T., Kim, J. W., Cho, J. G., Koo, J. S., Kang, S., and Jeong, R., 2016, "A Study on Suspension Optimization of the Korean Personal Rapid Transit Vehicle," *Trans. of the KSME(A)*, Vol. 40, No. 3, pp.317~326.

(2) Jeon, C. S., 2025, "A Study on the Dynamic Behavior of Newly Developed Dampers for High-speed EMU," *JKAIS*, Vol. 26, No. 1, pp.752~759.

† Dongjun Han (1223han@gmail.com),　* Youngkeun Kim (ykkim@handong.edu)

This certifies that the bachelor's thesis is approved.

_____

Thesis Advisor: Ph.D. Young-Keun Kim

_____

The Dean of Faculty: Ph.D. Chong-Sun Lee

School of Mechanical and Control Engineering

Handong Global University

June 2025